Microanalyses of Structure, Composition, and Morphology of the Surfaces and Interfaces in LSM-Infiltrated LSCF Cathodes

Wentao Qin, Mingfei Liu, Matthew E. Lynch, Jong-jin Choi and Meilin Liu
Center for Innovative Fuel Cell and Battery Technology, MSE, GaTech

Introduction

One of the reasons that $La_xSr_{1-x}Co_yFe_{1-y}O_{3-\delta}$ (LSCF) based cathodes show much better performance than those based on $La_xSr_{1-x}MnO_{3-\delta}$ (LSM) is that LSCF has much higher ionic and electronic conductivities than LSM, significantly extending the active sites beyond the triple-phase boundaries (TPB) [1]. One obvious downfall for LSCF is that it reacts adversely with YSZ, which can be mitigated by the use of a buffer layer of doped-CeO_2 between LSCF and YSZ [2]. However, the catalytic activity of the stand-alone LSCF cathodes is likely limited by the surface catalytic properties. Further, the long-term stability of LSCF cathodes is a concern. In contrast, LSM is more chemically stable and may facilitate stronger oxygen adsorption than LSCF. Thus, it is hypothesized that the *performance* and *stability* of a porous LSCF cathode may be improved by the application of a thin coating of LSM through infiltration. Indeed, our results demonstrate that cells with a porous LSCF cathode infiltrated with a thin-film coating of LSM, SDC, and LCC displayed higher power output and better long-term stability over those without catalyst coating. However, it is not clear how the catalyst is distributed on LSCF, what the surfaces and interfaces look like, and how they evolve during annealing and operation. The objective of the study is to characterize the morphology, structure, and composition of the surfaces and interfaces in a catalyst-infiltrated LSCF cathode as prepared, after annealing under certain conditions, and after subjecting to typical fuel cell operating conditions. The microscopic information about surfaces and interfaces will then be correlated with the electrochemical behavior of the electrodes under similar conditions in order to gain critical insights into the mechanisms of performance enhancement and design of better electrodes.

Experimental

The LSCF cathode was prepared by tape-casting and punched to button cell size. A suspension-coated SDC buffer layer was used to bond the LSCF tape to YSZ, in order to avoid reaction between LSCF and YSZ during the firing process. The LSCF cathode and YSZ were co-fired at 1100ºC for 2 hours. LSM-infiltration into the LSCF cathode was carried out with water-based 8020LSM solution. We also prepared LSM thin films on a polished LSCF pellet to facilitate our understanding of the catalyst / backbone system. The LSCF pellet was prepared by dry-pressing powder of 6428LSCF followed by sintering. The LSM film was fabricated by a sol-gel process. First, LSM solution with the target composition of 8020LSM at 0.3M concentration was prepared, with 2-methoxyethanol and acetic acid as solvents, and strontium acetate and manganese acetate as metal organic precursors. The solution was spin-coated on the LSCF pellet at 3000 RPM, and subsequently fired at 900ºC for 1 hour. A schematic cross-section view of an LSM-coated LSCF pellet is shown in Figure 1. The sample was analyzed as-prepared (900ºC for 1 hour) and after annealing (at 850ºC for 900 hrs in air).

Figure 1. A schematic cross-section view of an LSM-coated LSCF pellet.

TEM samples were prepared by the Focused Ion Beam (FIB) in-situ lift-out technique, with the Hitachi NB-5000 Dual-Beam FIB System operated at 40 kV. A thin sliver of the dimension of 10 μm (width) × 3 μm (height) × 0.5 μm (thickness) was cut and lifted out from the bulk of the material. The sliver was subsequently bonded on one side to the copper grid by tungsten deposition, after which the sliver was further thinned to electron transparency prior to the TEM analysis. Figure 2 presents an SEM image that shows such a sliver being lifted out.

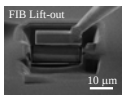

Figure 2. SEM image to illustrate lift-out of a sliver by a needle from bulk of the material

Microstructure characterization was carried out with a 300 kV HF3300 TEM/STEM/EDS. The TEM was equipped with a cold field-emission gun which provided a small electron probe of high electron current density. This was advantageous in the STEM/EDS operation mode, as the intense and fine probe could generate sufficient characteristic x-rays from small features. The STEM/EDS was performed with a probe size of about 1 nm and a take-off angle of 19.3 degrees. The live time set for each spectrum of a profile was 5 seconds.

Results and Discussion

Figure 3 (a) displays TEM images of an LSCF grain in a porous LSM-infiltrated LSCF cathode after operation at 0.7V and 750ºC for 900 hours. The inset presents a wider field of view of the grain. The grain is a single-crystal with the zone axis labeled in the image, and there is material that lacks long-range order of atom arrangement on the grain surface. Projected thickness of the surface material varies from 2 nm to 23 nm as labeled in the image. A representative HRTEM image of the bulk crystal is shown in Figure 3 (b). Figure 3 (c) is a Fourier-filtered image of the yellow squared area marked in (b), and where the zone-axis fringes of the LSCF crystal are labeled. It can be seen that after operation the grain retained the perovskite structure. Figure 3 (d) presents an HRTEM view of the surface of the LSCF grain, where the same zone-axis fringes are resolved and indexed in Figure 3 (e). The interface between the LSCF crystal and the surface material is well-defined as indicated by the abrupt termination of the zone-axis fringes of the LSCF crystal. An electron diffraction pattern acquired with the beam convergent on the surface material revealed radius of the first diffuse scattering ring to be 3.25 nm^{-1}, as shown in Figure 3 (f). The projected thickness of the surface coating is in the range of 2 nm to 16 nm. Figure 3 (g) and (h) display profiles of atomic percent across the surface layer along different directions. The sum of all the cation elements in each figure is normalized to 40%. The profiles in Figures 3 (g) and (h) show significant presence of Co at ~ 3%, Mn at 3 –10% and Sr at 4 – 9% in the surface layer. In short, the surface layer contains all the

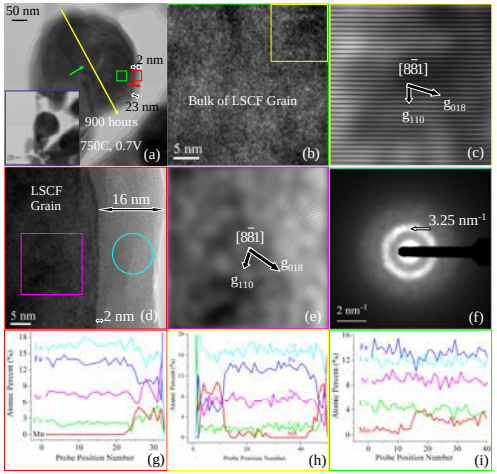

Figure 3. (a) TEM images of LSCF grain in the porous cathode infiltrated with water-based 8515LSM solution and after 900 hours of operation at 0.7V and 750ºC. The color squares mark areas that were zoomed in and displayed in (b) and (d). The color arrows denote profile lines. The inset provides a lower magnification image of the LSCF grain. (b) HRTEM image of the LSCF grain within the green square in (a). (c) Fourier-filtered image of the yellow square in (b). (d) HRTEM image of surface of the LSCF grain within the red square in (a). (e) Fourier-filtered image of the magenta square in (d). (f) Electron diffraction from surface layer within the blue circle in (d). Profiles of atomic percents associated with the red (g), yellow (h) and green (i) arrows in (a).

cation elements. Diffusion of Sr from the LSCF grain into the surface layer is likely since ~6% Sr shown in Figure (h) is higher than the nominal 4% in the LSM. On the other hand, Mn is limited to the surface layer. Figure 3 (i) reveals ~ 4% Mn 100 nm deep along the grain boundary (GB) of LSCF, implying that LSM might diffuse into LSCF along GBs.

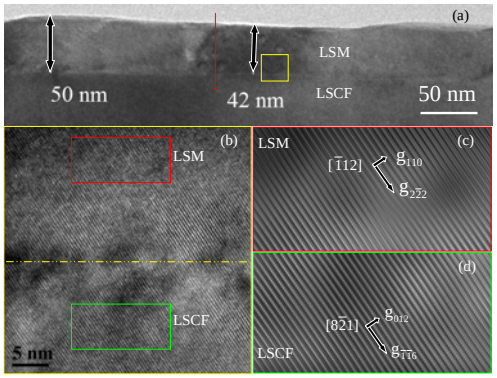

Figure 4 (a) A cross-sectional view of an LSM film (derived from a sol-gel process) on an LSCF pellet. The red arrow marks the profile line associated with profiles presented in Figure 6 (a). (b) HRTEM image of the LSM-LSCF interface. Approximate median of the interface is indicated by the broken yellow line. (c) and (d) Fourier-filtered images of the two phases near the interface, in the areas marked by the red and green rectangles in (a).

As shown in Figure 4 (a), the thickness of the LSM film ranges from 42 to 50 nm, which is consistent with the target thickness of 50 nm. The LSM layer appears crystalline. Figure 4 (b) presents HRTEM image of the LSM/LSCF interface. The broken yellow line in the figure labels approximate median of the interface. A structure coherence between the two phases is exhibited by the complete alignment of lattice fringes of the two phases at their interface. Crystallographic analyses indicate the LSM and LSCF are oriented along their zone axes, respectively. The zone axis images, processed after Fourier-filtering, are presented in Figure 4 (c) and Figure 4 (d).

Figure 5 (a) displays a cross-sectional view of the LSM/LSCF after annealing at 850ºC for 900 hours. There is no appreciable thickness change of the LSM film after annealing. Nonetheless, the top 80% of the film has lost long-range order as indicated by electron diffraction pattern shown in (c), and verified by the Z-contrast image in (b). The bottom 10 nm of the film and the underlying LSCF retain their respective perovskite structures, as well as the epitaxial relationship of the former to the latter, which are manifested by the lattice information presented in Figures 5 (d) to (f).

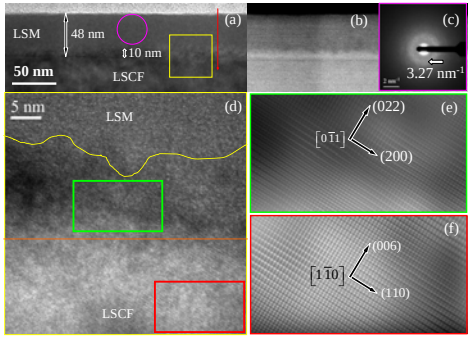

Figure 5 (a) TEM image of sol-gel LSM on LSCF pellet after annealing at 850 C for 900 hours. The red arrow marks the profile line associated with profiles presented in Figure 6 (b). The purple circle illustrates area for electron diffraction whose pattern is presented in (c). (b) Z-contrast image of the stack. (d) HRTEM image of the LSM/LSCF interface. Approximate boundary of lattice fringes in LSM is marked by the dashed yellow curve. (e) and (f) are Fourier-filtered images of the two phases near the interface, in the areas marked by the green and red rectangles, respectively, in (d).

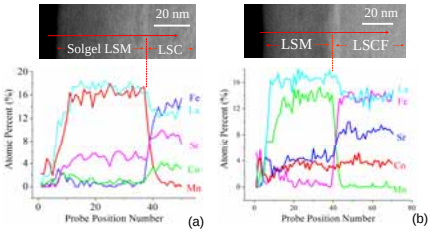

Figure 6. (a) Profiles of atomic percents associated with profile line marked by the red arrow in Figure 4(a), and (b) similarly 5(a).

Figure 6 (a) presents profiles across the LSM layer as prepared. The elemental distributions are consistent with stoichiometries of LSM and LSCF. After annealing, 3% of Co is present throughout thickness of the film, as shown in Figure 6 (b). Similar to profiles shown in Figures 3 (g) and (h), Mn is limited to the LSM layer.

Summary

A thin and amorphous surface layer was observed on the LSCF grain of LSM-infiltrated cathode after operation. This layer contains Co and Fe, in addition to La, Sr and Mn. Mn is confined within the surface layer and not observed in the underlying LSCF. The LSCF grain retains the perovskite structure. These observations are consistently verified by analyses of the LSM/LSCF interfaces before and after annealing/operation. Sr enrichment on surface of the LSCF was proposed as a cause of LSCF performance degradation [2 - 4]. We do not observe such Sr-enrichment on the LSCF grain of the LSM-infiltrated cathode after operation, which might have been inhibited by the LSM. This mechanism would slow down or eliminate degradation of cathode performance. LSM has been reported to possess higher binding energy of oxygen to the surface [5], hence stronger adsorption of O_2 than LSF or LSC. Consequently, a thin coating of LSM on LSCF is expected to facilitate O_2 adsorption. After operation, the LSM develops into a thin layer of LSCFM. Enhanced adsorption onto the surface layer is maintained because of the continued presence of Mn ions. Meanwhile, the reduced regularity of atom arrangement favors oxygen ion conductivity. The small thickness of the LSCFM layer is expected to further ease oxygen transport limitations through this surface layer.

Research Plan

We have designed a matrix of samples for a systematic approach to unraveling the mechanisms of performance and stability improvements by LSM coating. Further characterization will be conducted on other samples in the matrix including blank LSCF cathodes as prepared, after annealing, & after operation under typical fuel cell conditions. Also, the evolution of structure, composition, and morphology of LSM & LSCF surfaces and interfaces under fuel cell operating conditions will be acquired and correlated with electrochemical behavior in order to gain insights into rational design of better cathodes.

References

1. S. P. Jiang, *A comparison of O-2 reduction reactions on porous (La,Sr)MnO3 and (La,Sr)(Co,Fe)O-3 electrodes*. Solid State Ionics, 2002. **146**(1-2): p. 1-22.
2. S. P. Simner, M. D. Anderson, M. H. Engelhard, and J. W. Stevenson, "Degradation Mechanisms of La–Sr–Co–Fe–O SOFC Cathodes", Electrochemical and Solid-State Letters, 9(10) A478-A481, 2006.
3. Li, S.G., et al., *Tubular lanthanum cobaltite perovskite type membrane for oxygen permeation*. Journal of Membrane Science, 2000. **166**(1): p. 51-61.
4. Thursfield, A. and I.S. Metcalfe, *Air separation using a catalytically modified mixed conducting ceramic hollow fibre membrane module*. Journal of Membrane Science, 2007. **288**(1-2): p. 175-187.
5. Choi, Y., M.C. Lin, and M. Liu, *Rational design of novel cathode materials in solid oxide fuel cells using first-principles simulations*. Journal of Power Sources, 2010. **195**(5): p. 1441-1445.

Acknowledgement

The work is supported by US DOE SECA Core Technology Program under Grant No. DE-NT-0006557. We thank SHaRE, ORNL for TEM instrumentation and sample preparation.